Article

Journal of Industrial Textiles

0(0) 1–18

DOI: 10.1177/1528083719830144
journals.sagepub.com/home/jit

SAGE

Rheological response and quasi-static stab resistance of STF/MWCNTs-impregnated aramid fabrics with different textures

Ting-Ting Li[1,2], Xixi Cen[1], Haokai Peng[1,2], Haitao Ren[1], Lianhe Han[1], Ching-Wen Lou[1,2,3,4,5,6] and Jia-Horng Lin[1,2,4,6,7,8,9]

Abstract

Terrorist attacks occur constantly, which subsequently arouses awareness of self-protection. In order to alleviate the harm caused by sharp objects of knives and daggers, a design of flexible stab-resistant materials that are impregnated with the shear thickening fluid (STF)/multi-walled carbon nanotubes (MWCNTs) system and different texture of fabrics is presented. STF/MWCNTs are composed of polyethylene glycol (PEG 200) as the dispersion medium and silica (SiO_2) of 12 nm and 75 nm as disperse phase as well as MWCNTs as supplementary reinforcement, in expectation to provide the aramid fabrics with high strengths, low critical shear rate, and a short thickening response time. The textures of aramid fabrics—plain (P), twill (T), satin (S), or basket (B) weave—are

[1]Innovation Platform of Intelligent and Energy-Saving Textiles, School of Textiles Science and Engineering, Tianjin Polytechnic University, Tianjin, China
[2]Tianjin and Ministry of Education Key Laboratory for Advanced Textile Composite Materials, Tianjin Polytechnic University, Tianjin, China
[3]Department of Bioinformatics and Medical Engineering, Asia University, Taichung
[4]Fujian Key Laboratory of Novel Functional Textile Fibers and Materials, Minjiang University, Fuzhou, China
[5]Department of Medical Research, China Medical University Hospital, China Medical University, Taichung
[6]College of Textile and Clothing, Qingdao University, Shandong, China
[7]Laboratory of Fiber Application and Manufacturing, Department of Fiber and Composite Materials, Feng Chia University, Taichung
[8]School of Chinese Medicine, China Medical University, Taichung
[9]Department of Fashion Design, Asia University, Taichung

Corresponding author:
Jia-Horng Lin, Fujian Key Laboratory of Novel Functional Textile Fibers and Materials, Minjiang University, Fuzhou 350108, China.
Email: jhlin@fcu.edu.tw

saturated in the STF/MWCNTs system. The synergetic influences of silica size and texture on tensile strength, quasi-static knife, and spike stab resistances of the STF/MWCNTs-impregnated aramid fabrics are examined. Results show that the plain aramid fabric immersed in the STF/MWCNTs system containing 12 nm SiO_2 (SM12) exhibit the maximum tensile strength and quasi-static knife stab resistance, 14.7 MPa and 8.9 MPa, respectively, which is 1.15 and 1.43 times higher than pure aramid fabrics. Moreover, the basket-weave aramid fabric immersed in the STF/MWCNTs system containing 12 nm SiO_2 have the maximum quasi-static spike stab resistance of 17.12 MPa compared to other textures of fabrics, which is 1.05 times higher than those immersed in the 75 nm SiO_2 STF/MWCNTs (SM75) system and 1.33 times higher than that of pure basket aramid fabrics.

Keywords
Technical textiles, high-performance fabrics, fabrication weaving, shear thickening fluid, quasi-static stab resistance, protective fabrics

Introduction

People pay increasingly intensive attention to personal safety, which extends development and applications of individual protective products [1–3]. In particular, the popular stab-resistant flexible clothings that are soaked in a shear thickening fluid (STF) not only meet the primitive requirements of being light, soft, comfortable, and flexible but also have extraordinary impact resistance and stab resistant. STF has a reversible non-Newtonian fluid behavior and is commonly composed of a dispersion medium and a material at a disperse phase [4,5]. The shear thickening behaviors of STF are principally characterized by the viscosity and the rate of critical shear thickening. Once the shear rate or shear stress reaches the critical value, the balance of the system is sabotaged and the mobility of the system is prevented, resulting in greater viscosity [6,7]. When the shear rate or shear stress gradually decreases, the viscosity returns to its initial value [8]. In short, applying an external force to STF-impregnated high-performance fabrics can transform STF from a fluid state to a solid state. This transformation enhances the impact resistance of the fabric. STF was first found in hard ball type dispersions and named in 1938, after which the US military laboratory and Dr. Wetzel cooperated to develop bulletproof and flexible system armors [9]. Lee studied the SiO_2/PEG 200 STF-impregnated Kevlar fabrics and found that the energy absorption of the composite was proportional to the volume of STF [10]. In addition, Kalman et al. examined how the STF system composed of PMMA or SiO_2 at a dispersion phase influenced the protective properties of the fabrics. The test results indicated that regardless of whether it was PMMA or SiO_2 that comprised the STF, the STF-impregnated fabrics exhibited good spike stab resistance [11]. There have been many fruitful studies on STF protective materials; however, it remains difficult to have proper raw materials, concentration of STF, and content ratio of

STF that are compatible with spike/knife stab resistant and dynamic STF composites [10,11].

Multi-walled carbon nanotubes (MWCNTs) have become a focus in the fields of chemistry, physics, and materials due to the unique structure and mechanical and electrical properties [12–14]. MWCNTs also have high strength, high modulus, low density, and high band absorbent width and progress to a breakthrough being used in the nanoelectronic devices and super composite materials [15,16]. MWCNTs were first discovered in 1991 by Lijim in NEG Corporation of Japan, and its synthesis and purification technology has made great progress [17]. Given the numbers of graphite layers, carbon nanotubes can be divided into single-walled, double-walled, and multi-walled carbon nanotubes, the latter of which has a diameter of 5–20 nm and a length at a micron scale [18,19].

Moreover, para-aramid fiber as an aromatic polyamide fiber has many advantages such as high strength, high modulus, and high temperature resistance and is usually used in protective fields [20,21].Therefore, in this study, STF/MWCNTs systems with a good dispersion, low critical shear rate, and a short thickening time are formed using SiO_2 (12 nm and 75 nm) as a dispersion phase and MWCNTs as reinforcement after mechanical stirring and ultrasonic oscillation. The para-aramid textiles with plain (P), twill (T), satin (S), and basket (B) textures are separately immersed in the STF/MWCNTs systems. Tensile strength, quasi-static knife stab, and spike stab tests of STF/MWCNTs-impregnated fabrics are conducted to seek for optimal manufacturing parameters and to investigate the effects of SiO_2 particle size and fabric texture on these properties.

Experimental

Material

PEG 200 (Tianjin Xingfu Fine Chemical Research Institute, China) has a chemical purity. SiO_2 (Guangzhou GBS High-Tech & Industry, China) has two sizes of 12 nm and 75 nm. Anhydrous ethanol (Tianjin Fuyu Fine Chemical, China) has a concentration of 99.7%. Multi-walled carbon nanotubes (MWCNTs; Shanxi Fuhong Mineral Products, China) have specifications that are summarized in Table 1. Para-aramid filaments (Sinopec Yizheng Chemical Fiber, China) have a fineness of 112 tex/500f, a tenacity of 128.9N, and an elongation at break of 2.49%.

Table 1. Specification of MWCNTs.

Density (g/cm^3)	Purity (wt%)	Real density (g/cm^3)	Specific surface area (m^2/g)	Resistivity (s/cm)	Inside diameter (nm)	Outside diameter (nm)	Length (μm)	Preparation
0.15	>95	2.1	>233	100	3–5	8–15	50	CVD

CVD: Chemical Vapor Deposition.

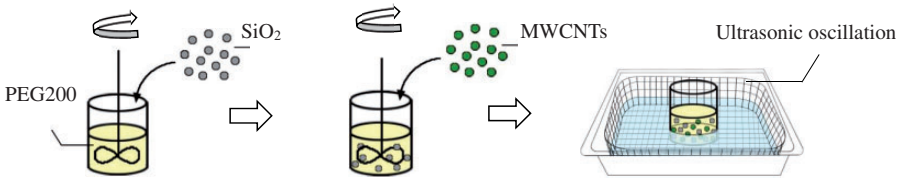

Figure 1. Process of the preparation of the STF/MWCNTs system. PEG: polyethylene glycol; SiO_2: silica; MWCNT: multi-walled carbon nanotube.

Preparation of samples

STF/MWCNTs systems: The STF is composed of polyethylene glycol (PEG 200) as the dispersion medium, silica (SiO_2) of 12 nm and 75 nm as the disperse phase, and MWCNTs are used as supplementary reinforcement. The process of STF/MWCNTs systems comprising 15% of SiO_2, 0.2% of MWCNTs, and 84.8% of PEG 200 is shown in Figure 1. PEG 200 firstly blended with 99.7% ethanol at a ratio of 1:2 at 100 rpm. SiO_2 with 12 nm or 75 nm is slowly mixed into the PEG/ethanol mixture by a mechanical stirring at 600 rpm for 2 h and then by an ultrasonic oscillation for 5 h in order to form the stable and uniform STF. Next, MWCNTs dispersed in 100 ml ethanol are then poured into the STF and ultrasonically oscillated for another 5 h, forming the STF/MWCNTs systems. Four kinds of STF and STF-MWCNTs systems, S12, S75, SM12, and SM75, prepared by the above process, are kept at the room temperature for 20 h and then dried in a vacuum dryer at 30°C for 8 h. Therein, S12 and S75 represent the STF containing 12 nm and 75 nm SiO_2, respectively; SM12 and SM75 represent the STF/MWCNT system containing 12 nm and 75 nm SiO_2, respectively.

STF/MWCNTs-impregnated aramid fabrics: A semi-automatic sample loom (DWL5016, Tianjin Longda Electromechanical Technology Development Co., Ltd., China) is used to fabricate the plain (P), twill (T), satin (S), and basket (B) aramid fabrics with warp and weft density of 130 counts/10 cm (Figure 2). The weaving loom with multi-arm blade opening has 50cm width and 16 healds.

The aramid fabrics in size of 180 mm × 25 mm and 100 mm × 100 mm were first dried in a vacuum drying oven at 150°C for 2 h, and then impregnated into the STF/MWCNTs systems after ultrasonic oscillation for 10 min. STF/MWCNTs-impregnated aramid fabrics were placed at room temperature for 24 h, and then compressed at 625 Pa, and finally air-dried for 24 h. The SEM images of different textures (1/1 P, 2/2 T, 5/3 S, and 2/2 B) of aramid fabrics impregnated with SM12 are observed by a scanning electron microscope (TM 1000, HITACHI, Japan) and are shown in Figure 3, and the morphology of the pure aramid fiber and aramid fibers impregnated with S12 and SM12 systems is observed by a scanning electron microscope (TM 3030, HITACHI, Japan) and is shown in Figure 4. Figures 3 and 4 confirm that the STF and STF/MWCNTs successfully impregnated on the

Figure 2. Textures of aramid fabrics: (a) 1/1 P, (b) 2/2 T, (c) 5/3 S, and (d) 2/2 B. P: plain; T: twill; S: satin; B: basket.

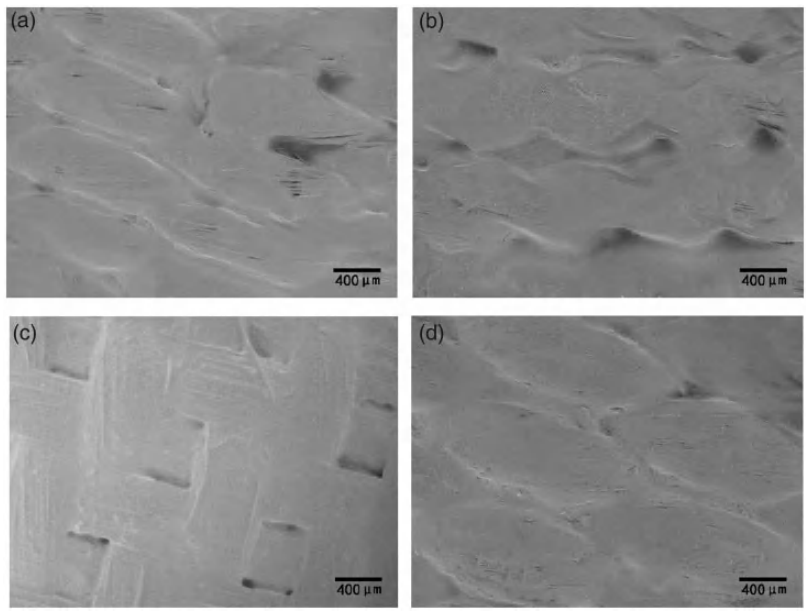

Figure 3. SEM of different textures (1/1 P, 2/2 T, 5/3 S, and 2/2 B) of aramid fabrics impregnated with SM12. P: plain; T: twill; S: satin; B: basket.

aramid fibers. The add-on amounts of STF/MWCNTs on fabrics aramid fabrics (P, T, S, and B) before and after impregnation are shown in Table 2.

Characterization and performance tests

Rheological response: The rheological response of the STF (S12 and S75) and STF/MWCNTs (SM12 and SM75) systems is measured by a Malvern rotational rheometer (Autosorb-1C, Malvern Instruments, UK) as shown in Figure 5. The plate has a diameter of 40 mm. The shear rate is between 0.1 and 1000 s^{-1}.

Tensile strength: A HT-2402 Universal Testing Machine (Hung Ta Instrument, China) is used to measure the tensile strength of the STF/MWCNTs-impregnated aramid fabrics as specified in ASTM D 5035-11 [22,23]. The experimental groups

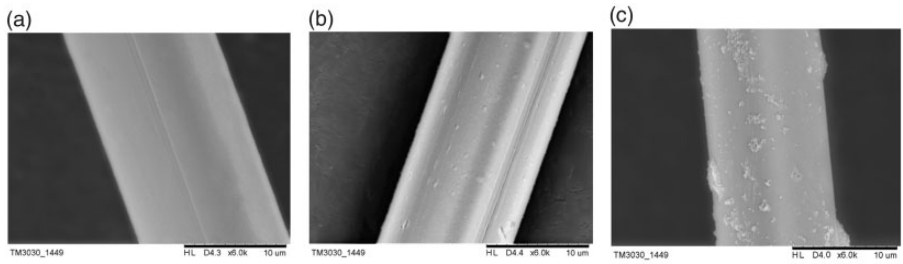

Figure 4. SEM images of (a) pure aramid fiber, and aramid fibers impregnated with (b) S12 and (c) SM12 systems.

Table 2. The add-on amounts of STF/MWCNTs of aramid fabrics before and after impregnation.

Fabric type weight	Before impregnation (g/100 cm^2)	After impregnation (g/100 cm^2)	Add-on amount (g/100 cm^2)
SM12			
P	1.68	6.92	5.24
T	2.02	7.11	5.09
S	2.17	7.36	5.19
B	2.43	7.79	5.36
SM75			
P	2.05	7.34	5.29
T	2.27	8.42	6.15
S	2.45	9.36	6.91
B	2.37	9.25	6.88

P: plain; T: twill; S: satin; B: basket.

are SM12 and SM75 aramid fabrics. The control group is pure aramid fabrics. Each sample has a size of 180 mm×25 mm. The tensile rate is 200 mm/min, the distance between clamps is 76 mm, and the breakpoint ratio is 5%.

Quasi-static knife/spike stab resistance: According to GA68-2008, STF/MWCNTs-impregnated aramid fabrics (SM12 and SM75) are tested for quasi-static knife or spike stab resistance using an Universal Testing Machine (Hung Ta Instrument, China) equipped with the knife or the spike stabs as seen in Figure 6 [24]. The control group is pure aramid fabrics. Each specification has three samples and samples are trimmed into 100 mm × 100 mm. The tensile rate is 200 mm/min and the breakpoint ratio is 5%.

Figure 5. The malvern rotational rheometer.

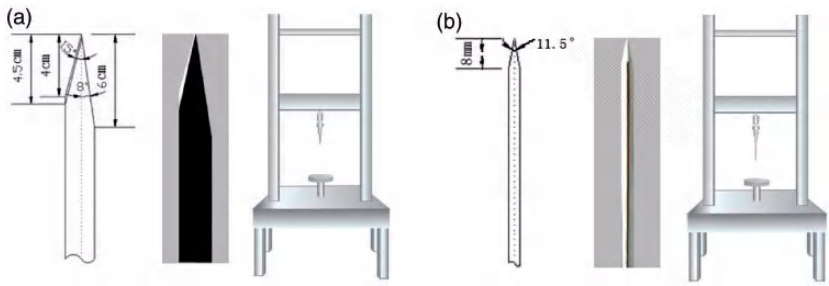

Figure 6. Specifications of (a) the knife stab and (b) the spike stab.

Results and discussion

Rheological properties of four shear thickening systems

Figure 7 shows the rheological properties of STF and STF/MWCNTs systems (S12, S75, SM12, and SM75). The four systems have a viscosity that undergoes three stages of shear thinning, thickening, and thinning. Based on the particle transition mechanism proposed by Hoffman, a low shear rate increases the degree of order of the particles, which has a negative influence on the viscosity of the system [25]. Increasing the shear rate strengthens the fluid force that is exerted on the particles. When the shear rate reaches the critical point, the particles have a random order, enhancing the viscosity of the system [25–27]. Based on the particle cluster mechanism proposed by Brady and Bossis G, a low shear force

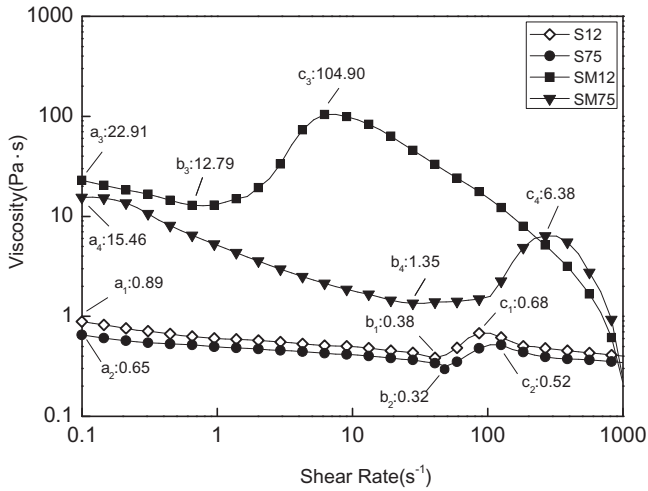

Figure 7. The steady-state rheological curves of the STF and the STF/MWCNTs systems as related to the particle size of SiO_2 and the addition of MWCNTs.

effect causes the particle to be arranged with a high degree of order, forming a stratiform structure and a thinner viscosity of the system [28,29]. Increasing the shear rate allows the hydrodynamic force to exceed the repulsion between particles, which increases the viscosity of the system [30]. Moreover, the initial viscosity (point a) and the maximum viscosity after thickening effect (point c) of the STF and the SM12 are greater than S75 and SM75. But the critical shear rate of SM12 is lower, which is ascribed to the averagely smaller particle size. At the same mass basis, 12 nm SiO_2 is smaller than 75 nm SiO_2, and there is thus a greater number of small-sized particles in the system, which contributes to a more frequent reaction among particles and an obvious shear thickening response. In addition, the MWCNTs also have an influence on the rheological properties of the STF. The addition of MWCNTs provides the STF/MWCNTs system with a higher viscosity and significant shear thickening effect. This is because MWCNTs have a long tubular structure and can be agglomerated around SiO_2 particles. However, the internal force between MWCNTs and PEG is lower which increase the slip of them. Consequently, the obvious phase separation is generated and thereby the shear thickening behavior is enhanced. For the SM12, the initial shear rate of the system is $0.1\,s^{-1}$ and the corresponding viscosity of the system is 22.91 Pa·s (a1). The viscosity of the system has a declining trend as a result of the increasing shear rate. In particular, the minimum viscosity of 12.79 Pa·s (b1) occurs when the critical shear rate is $0.79\,s^{-1}$. Afterwards, when the shear rate is $7.5\,s^{-1}$, the viscosity of the system rapidly increases and the viscosity reaches the maximum as 104.90 Pa·s (c1). The maximum viscosity of the SM12 is 9.49 times greater than SM75, and 33.29 times greater than S12. Moreover, the critical shear rate of the SM12 is 73.17% lower than SM75, and 81.58% lower than S12. The results indicate that the

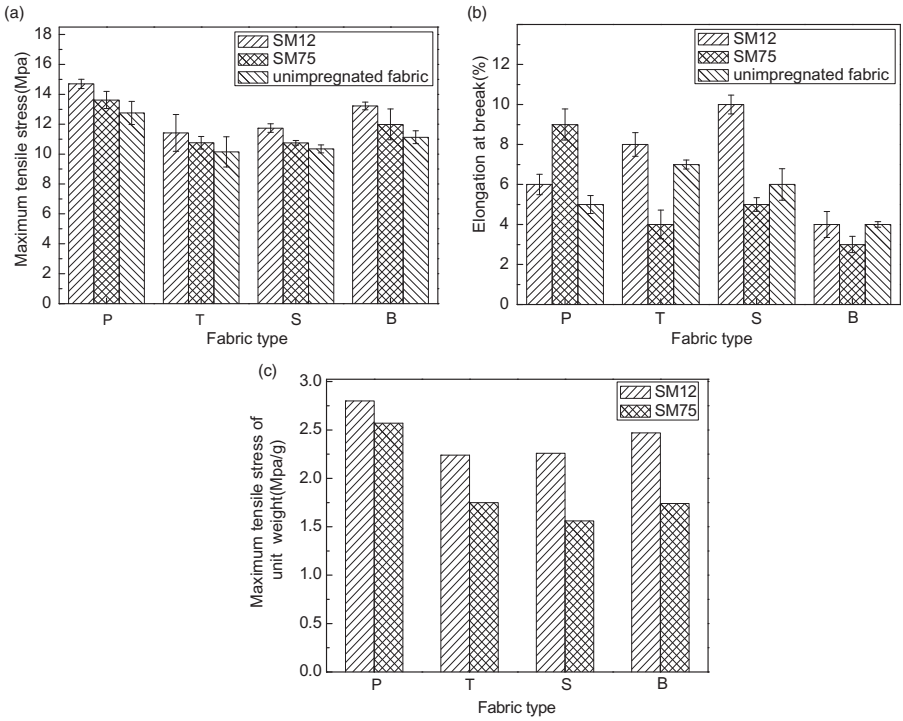

Figure 8. (a) The maximum tensile stress, (b) strain, and (c) normalized maximum tensile stress of the STF/MWCNTs-impregnated aramid fabrics as related to the size of SiO_2 and the texture of the fabrics.

addition of MWCNTs expedites the generation of particle clusters and then the critical shear rate.

Tensile strength and mechanisms of STF/MWCNTs-impregnated aramid fabrics

Figure 8(a) and (b) shows the effects of particle sizes of SiO_2 and texture of fabrics on the tensile properties of the STF/MWCNTs-impregnated aramid fabrics. Comparing to the control group (i.e. pure aramid fabrics), the STF/MWCNTs-impregnated aramid fabrics have greater maximum stress. Namely, the tensile properties of STF/MWCNTs-impregnated aramid fabrics are improved.

Plain aramid fabrics impregnated with SM12 have a maximum stress and strain that are 15.20% and 20% greater than those of the pure aramid fabrics. Similarly, plain aramid fabrics impregnated with SM75 have a maximum stress and strain that are 6.74% and 80% greater than those of the pure aramid fabrics. The results are ascribed to the transformation of STF/MWCNTs system. The STF/MWCNTs systems transform into a solid phase as a result of the impact of an external force,

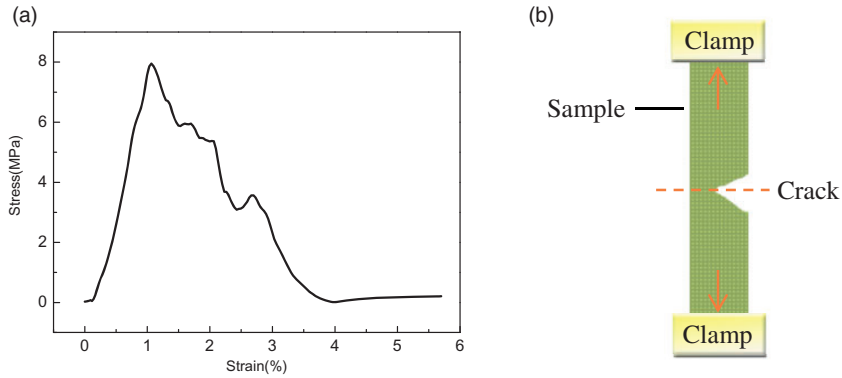

Figure 9. (a) The tensile stress–strain curves of STF/MWCNTs plain aramid fabrics. The particle size is 12 nm. (b) The fractured sample diagram after the tensile property measurement.

which restricts the slip of fibers and fiber bundles. Subsequently, STF/MWCNTs-impregnated plain aramid fabrics have improved tensile strength and are thus characterized with greater tensile properties [31].

For different SiO_2 size, the SM12 has a greater viscosity than SM75. A higher viscosity generates a greater cohesion, strengthening the tensile properties. Namely, the SM12 has greater viscosity that provides the plain aramid fabrics with higher tensile strength. Figure 8(a) also shows that for different texture of fabrics, STF/MWCNTs-impregnated aramid fabrics, plain aramid fabrics have greater stress than twill, satin, or basket aramid fabrics. The twill and satin aramid fabrics have comparable stress. The plain aramid fabrics used as the substrate can effectively enhance the tensile properties because the plain fabrics have closely related interlacing points. The more the interlacing points, the more stabilized the fabric structure. With the same add-on amounts of STF, the maximum tensile stress of STF/MWCNTs-impregnated aramid fabrics is normalized in Figure 8(c) according to (where σ_1 is the maximum tensile stress in Figure 8(a), σ_2 is the normalized maximum tensile stress, and G is the add-on amounts (g) in Table 2). The trend of normalized tensile stress as related to SiO_2 size and fabric texture is in conformity to that of maximum tensile stress in Figure 8(a), which shows that SM12-impregnated plain aramid fabrics have the best tensile strength.

Figure 9 shows the tensile stress–strain curves of the STF/MWCNTs plain aramid fabrics, and the particle size of SiO_2 is 12 nm. When enduring an external force, the aramid fabrics demonstrate deformation which is primarily ascribed to the extension of macromolecular chains of fibers. The tensile deformation consists of the bond length and angle, and can be plotted into a lasting smooth curve that meets the Hooke law [32]. When the external force steadily increases, the macromolecular chains of the amorphous area start to change until overcoming the non-chemical bond to trigger further extension. In the meanwhile, some macromolecular chains may also be broken or dissociate from the irregular crystalline area. Due to the different breaking points of fibers and yarns, the stress curve

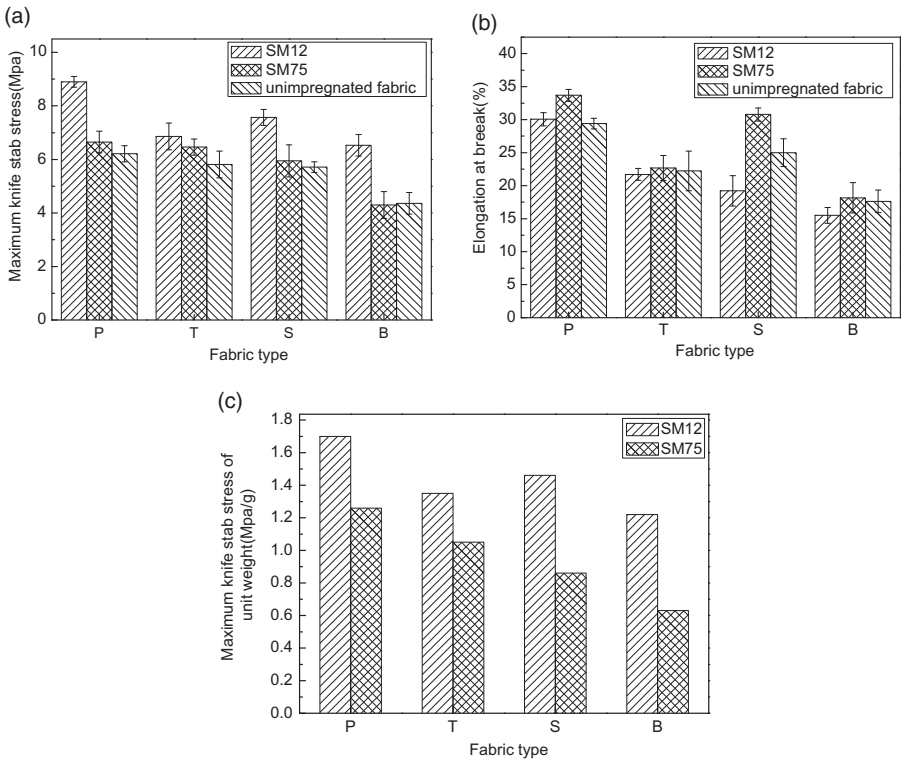

Figure 10. (a) The maximum quasi-static knife stab stress and (b) strain and (c) normalized maximum knife stab stress of the STF/MWCNTs-impregnated aramid fabrics as related to the size of SiO_2 and the texture of the fabrics.

fluctuates with the maximum stress and corresponding strain until the aramid fabrics break [33]. Then the stress value drastically drops as a result of the breakage of the aramid fabrics (Figure 9(b)).

Quasi-static knife stab resistance and mechanism of STF/MWCNTs-impregnated aramid fabrics

Figure 10(a) and (b) shows the influence of the particle size of SiO_2 and the texture of fabrics on the quasi-static knife stab resistance of STF/MWCNTs plain aramid fabrics. Moreover, STF/MWCNTs-impregnated plain aramid fabrics have greater knife stab resistance than that of pure plain aramid fabrics. With SM12, the maximum knife stab stress and strain are 43.32% and 2.28% greater than those of pure plain aramid fabrics. With SM75, the maximum knife stab stress value and strain value are 7.09% and 14.59% greater than those of pure plain aramid fabrics. The STF/MWCNTs immersion enables the aramid fabrics to endure the pierce because the SiO_2 particles at a disperse phase agglomerate to form solid matter, which in

turn restricts the slip of fiber bundles and fibers. Therefore, the aramid fabrics have greater knife stab resistance [34]. As far as the particle size is concerned, S12 provides the STF/MWCNTs system with greater maximum stress than S75. S12 can generate greater viscosity than S75, which efficiently improves the knife stab resistance of the STF/MWCNTs-impregnated plain aramid fabrics. As far as the texture of the fabric is concerned, the STF/MWCNTs-impregnated plain aramid fabrics have the highest maximum stress. When used as a matrix of the STF/MWCNTs-impregnated aramid fabrics, the plain texture has the most interlaced points, making the warp and weft yarns to be woven compactly, and thus creates the greatest knife stab resistance. Figure 10(c) shows the normalized maximum knife stab stress of the STF/MWCNTs-impregnated aramid fabrics as related to the size of SiO_2 and the texture of the fabrics. The normalized maximum knife stab stress at unit add-on amount is defined as the similar to the normalized tensile stress. The trend of the normalized knife stab stress conforms well to that of tensile strength as seen in Figure 10(a), which can be explained by the fact that yarn fracture becomes the main knife resistance mechanism. Moreover, Figure 10(a) also shows that SM12-impregnated plain aramid fabrics have the greatest knife stab resistance property.

Figure 11 shows the knife stab stress–strain curve of STF/MWCNTs-impregnated plain aramid fabrics. The maximum knife load of composite fabrics is 36.33 N at displacement of 17.30 mm, corresponding to 0.63J knife resistance energy. Basically, a knife stab can be divided into a shear force perpendicular to the fabric and a stretching force parallel to the fabric. When the knife impacts on the fabric, the fabric is deformed, and meanwhile, the shear thickening behavior of the STF/MWCNTs system dissipates some impact energy [35]. The knife stress value resultantly increases with the strain. As the knife continues to penetrate, the fabric around the knife tip begins to break forming crack. The fibers gradually accumulated near the crack, and then the fibers contacting with knife blade fractured. As the knife blade deepens, the above process is repeated and simultaneously

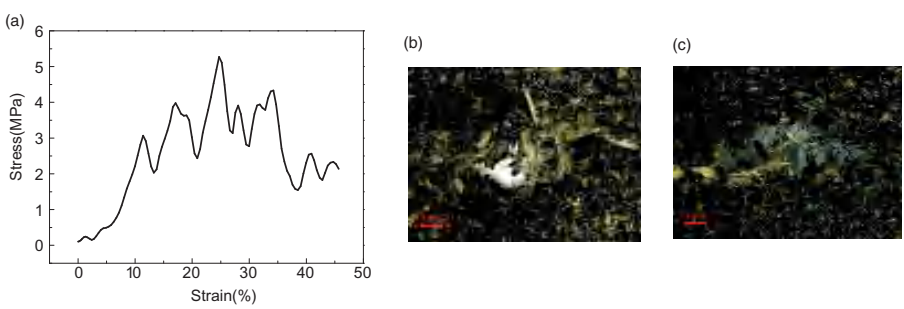

Figure 11. (a) The knife stab stress–strain curve of STF/MWCNTs plain aramid fabrics. The particle size of SiO_2 is 12 nm. Images of (b) the front and (c) the back of the sample after the knife stab resistance test.

the knife stress value fluctuated until the crack reaches the maximum. Afterwards, the knife is no longer subjected to external forces, and the stress value drops sharply [36]. The maximum crack after knife stab can be confirmed by Figure 11(b) and (c) for SM12 plain aramid fabrics.

Quasi-static spike stab resistance and mechanism of STF/MWCNTs-impregnated aramid fabrics

Figure 12 shows the influence of the particle size of SiO_2 and the texture of the fabric on the quasi-static spike stab resistance of the STF/MWCNTs-impregnated plain aramid fabrics. The spike stab resistance of STF/MWCNTs-impregnated plain aramid fabrics is higher than that of pure aramid fabrics. Comparing to the pure plain aramid fabrics, an immersion in SM12 provides the STF/MWCNTs-impregnated plain aramid fabrics with a 15.78% higher maximum stress and 4.29% higher maximum strain. Similarly, an immersion in SM75 provides the STF/MWCNTs-impregnated plain aramid fabrics with an 11.12% higher

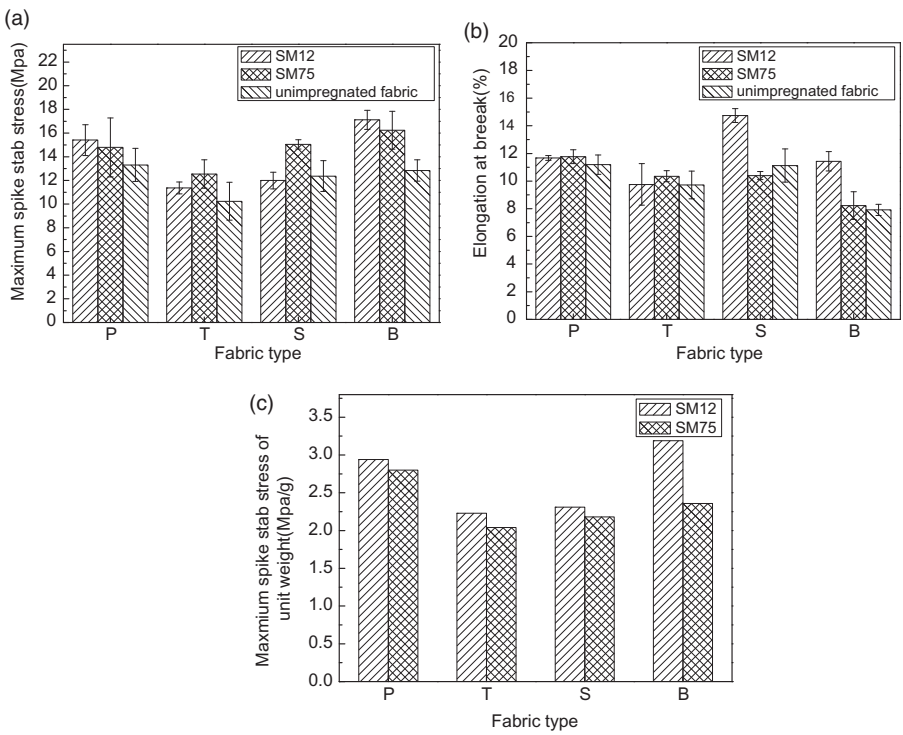

Figure 12. (a) The maximum quasi-static spike stab stress and (b) strain and (c) normalized maximum spike stab stress of the STF/MWCNTs-impregnated aramid fabrics as related to the size of SiO_2 and the texture of the fabrics.

maximum stress and 5.09% higher maximum strain. The results show that the STF/MWCNTs system effectively improves the spike stab resistance of the aramid fabrics, which is ascribed to the STF/MWCNTs system containing SiO_2 at a disperse phase. The SiO_2 particles agglomerate to form particle clusters as a result of the impact of a spike. The resulting shear thickening behavior then decreases the slip of fibers and fiber bundles and generates a greater friction against the spike, thereby improving the spike stab resistance [37]. For the plain aramid fabrics, the SM12 provides a higher spike stab resistance than SM75, but the opposite is the case for the twill and satin aramid fabrics. As far as the angle of textures is concerned, the STF/MWCNTs-impregnated basket aramid fabrics have a greater spike stab resistance than the STF/MWCNTs-impregnated plain, twill, and satin aramid fabrics. As far as the particle size of SiO_2 is concerned, the SM12 has a greater viscosity than SM75, which is beneficial to the cohesion between fiber bundles. Therefore, the SM12-impregnated basket aramid fabrics can withstand a greater shear force and demonstrate a greater spike stab resistance. Figure 12(c) shows the normalized maximum spike stab stress of the STF/MWCNTs-impregnated aramid fabrics as related to the size of SiO_2 and the texture of the fabrics. This normalized spike stab stress has consistent trend to knife stab stress and tensile strength. Furthermore, SM12-impregnated basket aramid fabrics have better spike stab resistance than other fabrics.

Figure 13 shows the spike stab stress–strain curve of the STF/MWCNTs plain aramid fabrics, and the particle size of SiO_2 is 12 nm. The maximum spike load is 193.04 N at displacement of 9.97 mm, corresponding to 1.92 J energy. When the spike first contacts the aramid fabrics, the STF/MWCNTs system efficiently thickens to maximize the friction among fiber bundles and fibers, prohibiting the spike from piercing the aramid fabrics [38,39]. As a result, the stress rises with an increase in the corresponding strain. The maximum stress (i.e. the highest external force that the fabrics can bear) occurs when the spike just pierces the fabrics. The friction among fiber bundles and fibers resists the penetration against the spike, during which the stress reaches the maximum, which is exemplified by the first peak in

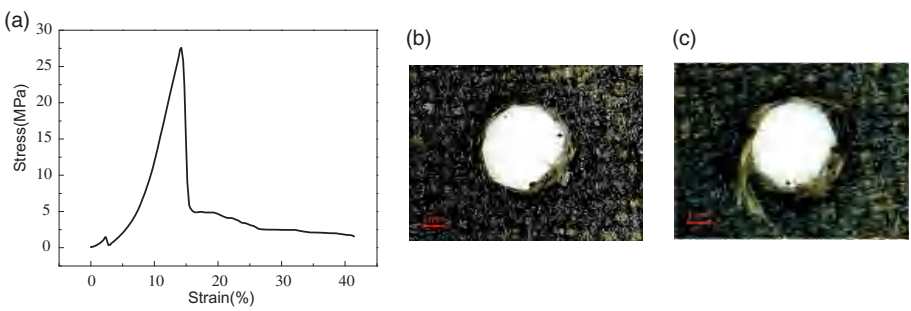

Figure 13. (a) The spike stab stress–strain curve of STF/MWCNTs plain aramid fabrics. The particle size of SiO_2 is 12 nm. (b) Images of the front and (c) the back of the sample after the spike stab resistance test.

Figure 13(a), and plummets subsequently. When the spike finally penetrates the fabric, the stress stops changing [40]. The biggest difference between the spike and the knife is that the knife has a blade on one side, which acts on the fabric to produce shearing force for cutting the yarn. However, when the spike acts on the fabric, the fiber bundle is squeezed around the spike, and the spike passes through between the bundles. At the same time, only a small part of the fiber filament breaks, which is the reason for the small fluctuation of the spike stress value compared with the knife. The damage of spike to the SM12 plain aramid fabrics is shown in Figure 13(b) and (c).

Conclusion

In this study, the stable STF/MWCNTs systems are formed using PEG 200 as the dispersion medium, 12 nm or 75 nm SiO_2 particles as disperse phase, and MWCNTs as reinforcement. Afterwards, plain, twill, satin, and basket weaving aramid fabrics are immersed in the STF/MWCNTs systems to make soft composite fabrics. The fabrics are tested for tensile strength, knife stab resistance, and spike stab resistance. The test results show that all of the four systems (S12, S75, SM12, and SM75) exhibit three stages as shearing shining, thickening, and then thinning. In particular, the SM12 has the highest initial viscosity, the highest viscosity after thickening, and the lowest critical shear rate among the four systems. The STF/MWCNTs-impregnated aramid fabrics have higher tensile strength and stab resistance than those of the pure aramid fabrics. Due to a greater viscosity, the SM12 provides the aramid fabrics with a higher knife stab resistance than SM75; with the same warp and weft density, the STF/MWCNTs-impregnated plain aramid fabrics have better tensile strength and greater knife stab resistance than other textured fabrics. The STF/MWCNTs-impregnated basket aramid fabrics have the highest spike stab resistance. This study explores the role of fabric textures and STF systems on stab resistance properties, and can be used for the design of soft stab-resistant body armor in the near future.

Declaration of conflicting interests

The author(s) declared no potential conflicts of interest with respect to the research, authorship, and/or publication of this article.

Funding

The author(s) disclosed receipt of the following financial support for the research, authorship, and/or publication of this article: The authors gratefully acknowledge the financial support provided by the Natural Science Foundation of Tianjin (18JCQNJC03400), National Natural Science Foundation of China (grant numbers 51503145 and 11702187), and the Open Project Program of Fujian Key Laboratory of Novel Functional Fibers and Materials (Minjiang University), China (No. FKLTFM 1704 and FKLTFM1722). This study is also supported by the Opening Project of Green Dyeing and Finishing Engineering Research Center of Fujian University (2017002B, 2017005B, and 2017001A).

ORCID iD

Ching-Wen Lou http://orcid.org/0000-0002-5448-6347
Jia-Horng Lin http://orcid.org/0000-0002-6913-8986

References

[1] Kang TJ, Chang YK and Hong KH. Rheological behavior of concentrated silica suspension and its application to soft armor. *J Appl Polym Sci* 2012; 124: 1534–1541.
[2] Lidén E, Berlin R, Janzon B, et al. Some observations relating to behind-body armour blunt trauma effects caused by ballistic impact. *J Trauma* 1988; 28: 145–148.
[3] Foy BE and Miner LH. Penetration-resistant aramid, Patent 5578358, USA, 1996.
[4] Majumdar A, Butola BS and Srivastava A. An analysis of deformation and energy absorption modes of shear thickening fluid treated Kevlar fabrics as soft body armour materials. *Mater Des* 2013; 51: 148–153.
[5] Khodadadi A, Liaghat GH, Sabet AR, et al. Experimental and numerical analysis of penetration into Kevlar fabric impregnated with shear thickening fluid. *J Thermoplast Compos Mater* 2018; 31: 392–407.
[6] Lim AS, Lopatnikov SL, Wagner NJ, et al. An experimental investigation into the kinematics of a concentrated hard-sphere colloidal suspension during Hopkinson bar evaluation at high stresses. *J Non-Newtonian Fluid Mech* 2010; 165: 1342–1350.
[7] Maurya SD, Purushothaman M, Krishnan PSG, et al. Effect of nano-calcium carbonate content on the properties of poly(urethane methacrylate) nanocomposites. *J Thermoplast Compos Mater* 2014; 27: 1711–1727.
[8] Gong X, Xu Y, Zhu W, et al. Study of the knife stab and puncture-resistant performance for shear thickening fluid enhanced fabric. *J Compos Mater* 2014; 48: 641–657.
[9] Sun LL, Xiong DS and Xu CY. Application of Shear Thickening Fluid in Ultra High Molecular Weight Polyethylene Fabric. *J Appl Polym Sci* 2013; 129: 1922–1928.
[10] Lee YS, Wetzel ED and Wagner NJ. The ballistic impact characteristics of Kevlar woven fabrics impregnated with a colloidal shear thickening fluid. *J Mater Sci* 2003; 38: 2825–2833.
[11] Kalman DP, Schein JB, Houghton JM, et al. Polymer dispersion based shear thickening fluid-fabrics for protective applications. *Proc SAMPE* 2007; 52: 1–9.
[12] Yu MF, Lourie O, Dyer MJ, et al. Strength and breaking mechanism of multiwalled carbon nanotubes under tensile load. *Science* 2000; 287: 637–640.
[13] Popov VN. Carbon nanotubes: properties and application. *Mater Sci Eng R* 2004; 43: 61–102.
[14] Wang ZL, Gao RP, Poncharal P, et al. Mechanical and electrostatic properties of carbon nanotubes and nanowires. *Mater Sci Eng C* 2001; 16: 3–10.
[15] Cao W, Song XM, Wang B, et al. Research progress of carbon nanotubes. *Mater Rev* 2007; S1: 77–82.
[16] Xu HJ, Zhang QZ, Jin FL, et al. Functionalization and application of multi-walled carbon nanotubes. *China Elastomerics* 2012; 22: 38–41.
[17] Dai H, Wong EW and Lieber CM. Probing electrical transport in nanomaterials: conductivity of individual carbon nanotubes. *Science* 1996; 272: 523–526.
[18] Iijima S. Helical microtubes of graphite carbon. *Nature* 1991; 354: 56–58.

[19] Falvo MR, Clary GJ, Nd TR, et al. Bending and buckling of carbon nanotubes under large strain. *Nature* 1997; 389: 582–584.
[20] Kong H, Zhang R, Zhou J, et al. Research status and progress of aramid fiber. *Mater China* 2013; 11: 676–684.
[21] Yuan JH, Jiang L, Ma JJ, et al. Application and development of aramid. *Hi-tech Fiber & Appl* 2005; 30: 27–30.
[22] Lu HN and Zhu HM. Comparison of differences in testing methods for tensile properties of textile strips. *Shanghai Text Sci Technol* 2006; 34: 41–44.
[23] Zuo XC, Zhang YP, Liu CS, et al. Individual stab material status and development trend. *Synth Fiber China* 2010; 39: 15–17.
[24] Ministry of Public Security Special Police Equipment Standardization Technical Committee. *GA 68-2008 Police stab-resistant clothing*. China: Standards Press of China, 2008.
[25] Wagner NJ and Brady JF. Shear thickening in colloidal dispersions. *Phys Today* 2009; 62: 27–32.
[26] D'Haene P, Mewis J and Fuller GG. Scattering dichroism measurements of flow-induced structure of a shear thickening suspension. *J Colloid Interface Sci* 1993; 156: 350–358.
[27] Bender JW and Wagner NJ. Optical measurement of the contributions of colloidal forces to the rheology of concentrated suspensions. *J Colloid Interface Sci* 1995; 172: 171–184.
[28] And VTO and Mackay ME. Stress components and shear thickening of concentrated hard sphere suspensions. *Langmuir* 2000; 16: 7931–7938.
[29] Bossis G and Brady JF. The rheology of Brownian suspensions. *J Chem Phys* 1989; 91: 1866–1874.
[30] Brady JF and Bossis G. Stokesian dynamics. *Annu Rev Fluid Mech* 1988; 20: 111–157.
[31] Hassan TA, Rangari VK and Jeelani S. Synthesis, processing and characterization of shear thickening fluid (STF) impregnated fabric composites. *Mater Sci Eng A* 2010; 527: 2892–2899.
[32] Qin J, Zhang G, Zhou L, et al. Dynamic/quasi-static stab-resistance and mechanical properties of soft body armour composites constructed from Kevlar fabrics and shear thickening fluids. *RSC Adv* 2017; 7: 39803–39813.
[33] Bilisik K. Properties of yarn pull-out in para-aramid fabric structure and analysis by statistical model. *Compos A* 2011; 42: 1930–1942.
[34] Fu K, Wang H, Wang S, et al. Compressive behaviour of shear-thickening fluid with concentrated polymers at high strain rates. *Mater Des* 2018; 140: 295–306.
[35] Salim Y, Yahya MY, Israr HA, et al. A review on stab and spike resistance performance of shear thickening fluids (STF) impregnated fabrics. In: *International conference on latest trends in engineering and technology*, Kuala Lumpur, Malaysia, 22–24 May 2017, pp. 37–42.
[36] Li TT, Zhang XY, Peng HK, et al. Thermally bonded PET–basalt sandwich composites for heat pipeline protection: preparation, stab resisting, and thermal-insulating properties. *Appl Sci-Basel* 2018; 8: 510.
[37] He Q, Cao S, Wang Y, et al. Impact resistance of shear thickening fluid/Kevlar composite treated with shear-stiffening gel. *Compos A Appl S* 2018; 106: 82–90.

[38] Cao S, Chen Q, Wang Y, et al. High strain-rate dynamic mechanical properties of Kevlar fabrics impregnated with shear thickening fluid. *Compos A Appl S* 2017; 100: 161–169.
[39] Joselin R and Wilson WJ. Investigation on impact strength properties of kevlar fabric using different shear thickening fluid composition. *Defence Sci J* 2014; 64: 236–243.
[40] Crawford NC, Williams SKR, Boldridge D, et al. Shear thickening and defect formation of fumed silica CMP slurries. *Colloids Surf A* 2013; 436: 87–96.